Marine Geology 299–302 (2012) 63–76

Contents lists available at SciVerse ScienceDirect

Marine Geology

journal homepage: www.elsevier.com/locate/margeo

Modeling the formation of a sand bar within a large funnel-shaped, tide-dominated estuary: Qiantangjiang Estuary, China

Qian Yu [a,b,*], Yunwei Wang [a], Shu Gao [a], Burg Flemming [b]

[a] MOE Laboratory for Coast and Island Development, Nanjing University, China
[b] Senckenberg Institute, Wilhelmshaven, Germany

ARTICLE INFO

Article history:
Received 31 May 2011
Received in revised form 13 December 2011
Accepted 27 December 2011
Available online 10 January 2012

Communicated by J.T. Wells

Keywords:
longterm morphological model
sand bar
Qiangtangjiang Estuary

ABSTRACT

The Qiangtangjiang Estuary (the outer part being known as Hangzhou Bay) located on the east coast of China is a large funnel-shaped, tide-dominated and well-mixed estuary. The equilibrium estuarine morphology has been attained and characterized by a large sand bar having a total length of 125 km and an elevation of 10 m above the average adjacent seabed. In order to investigate the physical processes governing the formation of this morphological feature, two-dimensional depth-averaged process-based morphodynamic modeling (Delft3D) was carried out on a schematized funnel-shaped domain with exponentially decreasing widths based on the dimensions of the Qiangtangjiang Estuary. The model simulated a 6000-year period, the output showing the development of a sand bar that reached equilibrium within about 3000 years. The general shape, size and position of the modeled sand bar are consistent with the observations. Short-term simulations of hydrodynamic and sediment transport processes at the initial stage indicate that, in response to the interactions between river discharge and tidal currents, which are strongly influenced by the funnel-shape, the sand bar developed in the transition zone between the river-dominated upper estuary and the flood-dominated lower estuary where sediment transport pathways converge. A series of sensitivity analyses suggest that the estuarine convergence rate, sediment grain size, and river discharge are the main controlling factors of sand bar formation. Similar to other large funnel-shaped, tide-dominated estuaries of the world, a sufficient supply of fine cohesionless sediment (derived from the adjacent Changjiang Estuary), a large river discharge, and a strong shoreline convergence rate have shaped the large sand bar in the Qiangtangjiang Estuary.

1. Introduction

In association with the decelerating sea-level rise during the Holocene, numerous morphological features developed along coasts where the sediment-laden freshwater of rivers met the salt water of the advancing sea (Stanley and Warne, 1994). The two most distinctive of these are deltas and estuaries. Deltas are recognized as discrete bulges in the shoreline where the associated rivers deliver more sediment than the rising sea can accommodate or marine processes can redistribute (Swift and Thorne, 1991; Bhattacharya, 2003). By contrast, where both fluvial and marine sediment supply are insufficient to fill the drowned river valleys, the river sections that experience marine influence are called estuaries (Dalrymple et al., 1992; Bhattacharya, 2003).

River discharge, tidal energy flux, and wave action are considered to be the three dominant processes controlling delta morphology (Galloway, 1975), and only a few modern examples of tidal dominated deltas have been documented, e.g., the Fly River delta, Papua New Guinea (Dalrymple et al., 2003; Harris et al., 2004). This concept can also be applied to estuaries, among which tide-dominated estuaries are characterized by strong tidal currents transporting more sediment than either river currents or waves (Wells, 1995). Several large tide-dominated estuaries have been studied in detail, e.g., the Cobequid Bay–Salmon River Estuary in the Bay of Fundy (Amos, 1978; Dalrymple et al., 1990), the Bristol Channel–Severn Estuary in western England (Harris and Collins, 1985; Harris, 1988; Allen, 1990), and the Wester Schelde estuary in the Netherlands (Toffolon and Crosato, 2007; van der Wegen and Roelvink, 2008; van der Wegen et al., 2008), and today form the basis for the generalized tide-dominated estuarine morphological and faces model conceptually defined by Dalrymple et al. (1992) and Dalrymple and Choi (2007). However, as noted by Dalrymple and Choi (2007), individual cases must be examined critically within the generalized concept.

The Qiangtangjiang Estuary (QE) on the east coast of China is one of such cases. It is a large funnel-shaped, tide-dominated and well-mixed estuary located just south of the Changjiang (Yangtze) Estuary (Figs. 1 and 2). The most significant morphological aspect is the presence of a large sand bar within the estuary between the laterally averaged longitudinal bed profile and the straight downstream trend (Fig. 3) (Chien et al., 1964). Because this large sand bar looks like a

* Corresponding author at: MOE Laboratory for Coast and Island Development, Nanjing University, China. Tel.: +86 25 83597308; fax: +86 25 83595387.
E-mail address: qianyu.nju@gmail.com (Q. Yu).

0025-3227/$ – see front matter © 2012 Elsevier B.V. All rights reserved.
doi:10.1016/j.margeo.2011.12.008

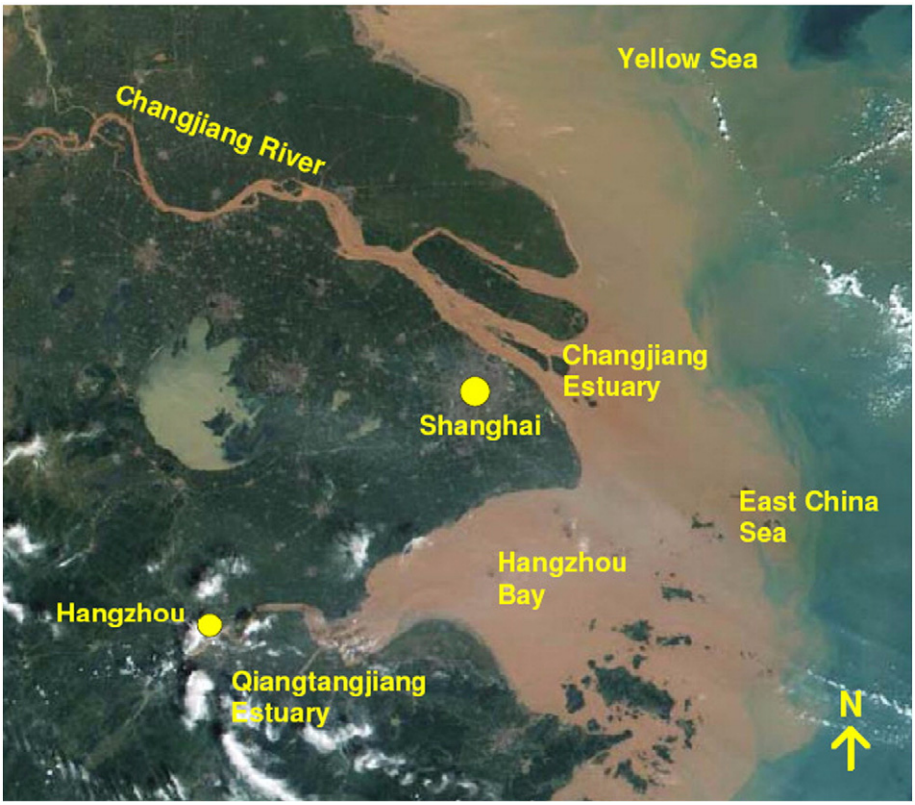

Fig. 1. Annotated satellite image showing the location of the Qiangtangjiang Estuary, Hangzhou Bay, and the Changjiang (Yangtze) River and Estuary along the east coast of China.

doorsill connecting the interior of a house (land) with the outdoor area (sea), it is called "sandy doorsill" in Chinese.

The historical evolution and dynamic processes forming the large sand bar were studied in the early 1960s by the evaluation of historical documents, morphological and sedimentological surveys, and hydrodynamic and sediment transport observations (Chen et al., 1964; Chien et al., 1964). On the basis of these data it was suggested that, following the formation of the funnel-shaped estuary, a large amount of sediment originating from the Changjiang River was transported into the estuary by the strong flood-dominated tidal currents to form the large sand bar. However, this hypothesis has to date not been verified by more quantitative investigations of these processes in combination with the influence of associated forcing factors such as sediment supply, river discharge, and estuary shape.

This problem not only applies to the QE, but also to most other large tide-dominated estuaries and, in particular, also to the generalized estuarine facies model. Being one of the most striking features of the overall estuarine morphology, such bulges (i.e. the large bars) above the straight, sloping bed trends have received surprisingly little attention. Although it is well-known that the bars form naturally as a consequence of the decrease in river power and the concomitant increase in the strength of the tidal current, little work has been carried out on the quantification of how the bars scale with the different forcing factors in the estuaries (Bhattacharya, 2003).

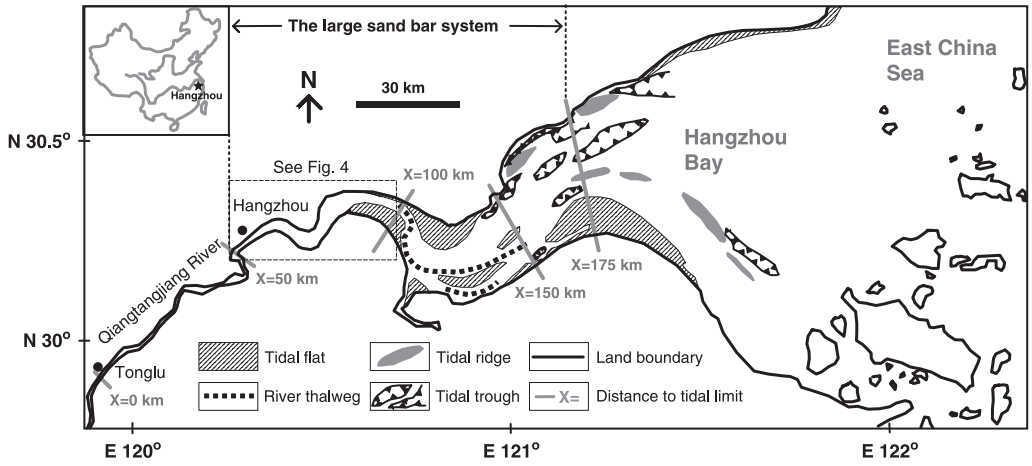

Fig. 2. Morphological map of the Hangzhou Bay-Qiantangjiang estuary.
Modified after Chen et al., 1964, and Feng et al., 1990.

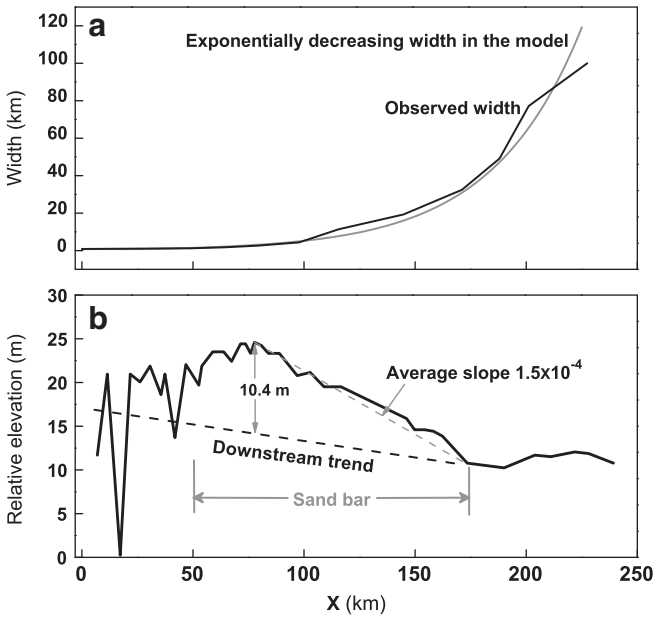

Fig. 3. (a) Comparison of the observed width of the Qiangtangjiang Estuary with the exponentially increasing width used in the numerical model as described by Eq. (1). (b) Observed average longitudinal bed profile of the Qiangtangjiang Estuary showing the large sand bar elevated above the mean bed slope trend downstream of Tonglu (see Fig. 2).
Modified after Chien et al., 1964.

In recent years, idealized analytical methods have been used to explain tide-dominated estuarine morphologies (e.g., Schuttelaars and de Swart, 2000; Prandle, 2004), but with increasing complexity, numerical models offer more information on system evolution, although they are generically not easily understood compared with analytical models (Dronkers, 2005). Due to the advantages in interpreting field observations and analyzing the sensitivity to different parameters, numerical modeling is considered a useful tool to study the morphodynamics of coastal systems (Dronkers, 2005; de Swart and Zimmerman, 2009). In the recent past, one-dimensional (1D) models have been solved numerically in order to assess the long-term morphological evolution and equilibrium of tide-dominated, well-mixed estuaries (Lanzoni and Seminara, 2002; Hibma et al., 2003b; Todeschini et al., 2008), the results emphasizing the crucial role of the convergence rate of the opposing estuarine shorelines on the longitudinal bed profiles. Applying newly developed three-dimensional numerical modeling techniques (Lesser et al., 2004; Roelvink, 2006), it has become possible to study long-term estuarine morphodynamics by means of two-dimensional, depth-averaged (2DH) process-based models (Hibma et al., 2003a; Montano and Carbajal, 2008; van der Wegen and Roelvink, 2008; van der Wegen et al., 2008). In this way it has been possible to reconstruct morphological evolution histories and to simulate the formation of channel and shoal patterns.

However, two important factors are not incorporated in the above modeling approaches. The first factor is sediment supply, including the rate and the character (e.g., cohesive properties and grain size) of sediment input from both the river and the open sea. This aspect is particularly important as sediment supply has been suggested as one of the key factors controlling estuarine and delta morphology (Harris, 1988; Swift and Thorne, 1991; Orton and Reading, 1993; Gao, 2007; van der Wegen et al., 2011). For example, the Bristol Channel–Severn Estuary is a typical sediment-starved estuary (Harris and Collins, 1985), whereas the sand composing the elongate tidal bar systems in the head section of the Cobequid Bay–Salmon River Estuary originated from the landward sorting of downstream glacial deposits (Dalrymple et al., 1990). In the case of the QE, a large contribution of cohesionless silt from the neighboring Changjiang River has been suggested by Chen et al. (1964) and Chien et al. (1964). However, most of the previously applied numerical models have merely assumed a fixed grain size and a sufficient sediment supply. Consequently, the morphological response of estuaries to different sediment supply conditions is still poorly understood.

River discharge is another important factor. van der Wegen (2010) modeled the Wester Schelde estuary morphology with a river discharge of 15 $m^3 s^{-1}$, but most of the previous models neglected it at the landward boundary assuming that it was much less than the prevailing tidal discharge. However, although tides dominate over most of an estuary, river discharge and sediment supply may play an important role at the landward end where smaller channel cross-sections and tidal prisms prevail (Perillo, 1995; Todeschini et al., 2008). As a result, the question on whether and how river discharge influences the estuarine morphology remains problematical, even if it is generally much smaller than the tidal discharge and the estuary remains well-mixed.

In view of this situation, the following questions may be raised in connection with the Qiantangtjiang Estuary: Focusing on the estuarine longitudinal bed profile, (1) how can the formation process of the large sand bar in the QE be quantitatively reconstructed, and (2), in comparison with other large tide-dominated estuaries, how can the effects of estuarine convergence, sediment supply and river discharge in the generalized estuarine morphological model be evaluated?

In the present contribution, an attempt is made to answer the above questions by applying a physically-based numerical modeling technique. Owing to the complexity of tide-dominated estuaries associated with interactions of numerous physical, chemical and biological processes, and irregular and variable boundary conditions (Wells, 1995; Dalrymple and Choi, 2007), the numerical modeling approach has been simplified to the extent that only key processes and configurations were considered, from which the first-order dynamics could be extracted and anomalous and idiosyncratic situations could be identified (Paola, 2011). By this approach it was hoped to obtain an improved understanding of the morphodynamics and the resulting morphology of large tide-dominated estuaries. It is emphasized that the present study only concentrates on the large sand bar along the laterally averaged longitudinal bed profile, and not on the estuarine infilling history (e.g., Lin et al., 2005) or the development of lateral channel and ridge patterns (e.g., Hibma et al., 2003a; Xie et al., 2009).

2. Study area

The QE is the biggest estuary along the East China Sea coast of China. The length of the estuary from the landward tidal limit to the estuarine mouth is around 250 km, and the width decreases steeply from 100 km at the mouth to around 1 km at the landward limit of tidal influence (Figs. 2 and 3a). The southern part of the wide mouth, which connects with the East China Sea, is protected by numerous small islands, while the northern shore converges on the southern tip of the outer Changjiang Estuary (Figs. 1 and 2).

The estuary can be divided into three morphological sections: an upper section from $x=0$ to $x=50$ km, a middle section from $x=50$ to $x=150$ km, and an outer section where $x>150$ km, the origin of the x-coordinate being located near the landward tidal limit (see Fig. 2, Chien et al., 1964; Lin et al., 2005). The upper section is a stable anabranching channel, which is dominated by fluvial processes. Due to the interaction of fluvial and tidal processes, the middle section is characterized by a shallow and wide estuarine bed with a laterally migrating channel thalweg lined by unstable intertidal flats. Fig. 4 illustrates the position of the thalweg in the upper part of the middle section recorded between March 1953 and December 1958, illustrating the pronounced lateral migration across the whole estuary. The marine dominated outer section is also called Hangzhou Bay where the strong

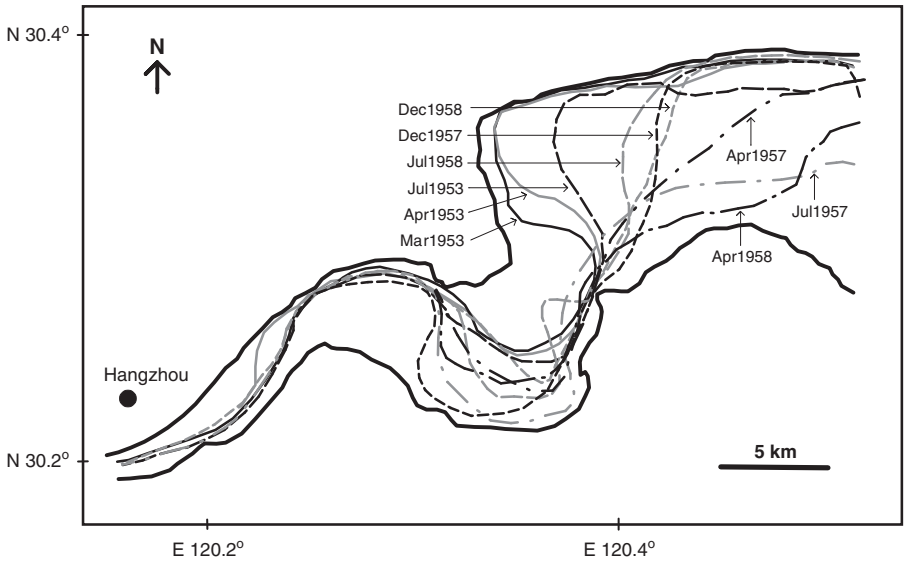

Fig. 4. Lateral migration of the channel thalweg recorded in the upper part of the middle section of the Qiangtangjiang Estuary (the area in marked in Fig. 2) between March 1953 and December 1958.
Modified from Chien et al., 1964.

tidal currents have formed a ridge and swale topography. Seaward of this the bed is relatively flat.

The most striking morphological feature of the QE is the presence of a large sand bar. Fig. 3b shows the laterally averaged longitudinal bed profile of the QE, along which the large sand bar can be clearly identified as a bulge above the straight downstream trend. The body of the large sand bar extends from $x = 50$ to $x = 175$ km, having a total length of around 125 km, a peak crest height of 10.4 m above the base line, and a front slope of 1.5×10^{-4}.

The longitudinal profile has been relatively stable from the 1910s to the 1950s, suggesting that the large sand bar has attained an equilibrium state (Chien et al., 1964). Recent observations indicate that, associated with intensified land reclamation over the past several decades, the estuary has generally experienced renewed infilling between 1981 and 2005 (Guo et al., 2009). On a longer time scale, Chen et al. (1964) have suggested that the basic shape of the sand bar has evolved around 2500 years BP, following the establishment of the funnel-shaped geometry of the QE some 1000 years earlier. After initiation, the sand bar gradually prograded seaward while growing in height. During this period, sea-level has remained stable (Chen and Stanley, 1998; Hori et al., 2001).

The Qiantangjiang River, the main source of freshwater and sediment to the QE, has the average water discharge of 952 $m^3 s^{-1}$ and the annual average river sediment flux of around 6 million tons, consisting mainly of coarse silt to fine sand (Chien et al., 1964; Pan and Huang, 2010). Most of the discharged sediment is trapped in the estuary and only the finest portion escapes into the East China Sea (Su and Wang, 1989). The adjacent Changjiang River, which has an average water discharge of 29,000 $m^3 s^{-1}$ and an annual average sediment flux of 486 million tons, is another major sediment source (Chen et al., 1964; Su and Wang, 1989).

The entire estuary is occupied mainly by well sorted fine-grained cohesionless sediment having median grain sizes between 20 and 40 μm, the clay component (finer than 4 μm) contributing less than 3%, which explains the cohesionless dynamic nature (Chen et al., 1964; Dyer, 1986; Zhou and Gao, 2004). The sediment can be classified as sortable silt, which is predominantly transported as single grains (McCave and Hall, 2006; Chang et al., 2007).

The tide is the main driving force in the QE, the dominant tidal component being the M2 constituent (ECCHE, 1992). According to the definition of Dyer (1997), the QE is a typical hypersynchronic estuary. Because of the funnel-shaped geometry, the average tidal range increases from 2–3 m at the mouth to more than 4 m at $x = 125$ km, after which the friction offsets the influence of convergence, causing the tidal range to progressively decrease to zero at the upper tidal limit (Zhou and Gao, 2004; Lin et al., 2005). The strong tidal influence destroys any vertical stratification to produce the well-mixed nature of the QE (Mao et al., 1964; ECICTZ, 1988). Because of the protection by islands at the mouth, the wave climate is dominated by local wind waves, mean annual wave heights decreasing from 0.5 m at around $x = 225$ km to 0.2 m at around $x = 175$ km, and even less in the middle and inner sections (Han et al., 2003).

3. Methods

3.1. Model description

In order to examine in detail how the large sand bar in the QE formed and what the influence of estuarine convergence, sediment supply and river discharge was on the longitudinal bed profile, a 2DH process-based morphodynamic model (Delft3D software package) was used. Delft3D has been utilized and validated widely in different coastal environments to simulate longterm morphodynamic changes on different time scales (e.g., Dastgheib et al., 2008; Edmonds and Slingerland, 2010; Yu et al., in press), including tide-dominated well-mixed estuaries (Hibma et al., 2003a; van der Wegen and Roelvink, 2008; van der Wegen et al., 2008). Xie et al. (2009) applied Delft3D to the QE, obtaining a reasonable similarity in the channel pattern when comparing the observational data with the results of a 30-year modeling period.

In the model, in accordance with the tide-dominated well-mixed characteristics, only tidal forcing and river discharge were considered, neglecting vertical velocities, density differences, as well as wind and waves (Dastgheib et al., 2008; van der Wegen and Roelvink, 2008; van der Wegen et al., 2008). On the other hand, the Coriolis force was taken into account in the model due to the large spatial scale. The 2DH continuity equation and nonlinear, shallow-water momentum equations for incompressible free surface flow are solved numerically with a constant seabed drag coefficient of 3×10^{-3} (Soulsby, 1997; Lesser et al., 2004).

Sediment transport is calculated by the van Rijn approach for single-size cohesionless grains (van Rijn, 2000). The standard

advection–diffusion equation is adopted for suspended sediment transport and the Exner equation is employed for both suspended load and bedload to simulate the morphological changes based on the sediment mass conservation law. When using multi-sized sediments, the same van Rijn approach and advection–diffusion equation were applied, but the reference concentration, erosion rate and sediment transport rate of each sediment fraction were considered proportional to the availability of each fraction on the bed (Guillou et al., 2009; van der Molen et al., 2009). The bed composition model was changed from a uniformly mixed bed (one sediment layer) for a single-size sediment to a multi-layer concept for multi-sized grains (Edmonds and Slingerland, 2010; Geleynse et al., 2010; van der Wegen et al., 2011). The model defines a transport layer with a fixed height of 0.1 m and a maximum number of 50 bookkeeping layers (each 0.2 m thick) to keep track of sedimentary stratigraphy. Net deposited sediment is initially added to and mixed into the top-most layer until the defined constant thickness of 0.2 m is exceeded, after which a new bookkeeping layer is created. When net erosion takes place, only sediment in the top-most layer is available. In this way, the bed armoring phenomenon can be simulated, which results in lag deposits composed of coarser sediment fractions that prevent the covered finer sediments from being eroded (Flemming et al., 1992; Wiberg et al., 1994; Reed et al., 1999).

As longterm modeling is demanded, the "online" approach is used to save calculation time (Roelvink, 2006; Ranasinghe et al., 2011). It speeds up bed adjustments by multiplying the bed sediment flux in each time step by a morphological scaling factor (MF). This method was successfully applied in longterm morphological modeling with a typical MF in the order of 100, e.g., Dastgheib et al. (2008) used an MF of 300, van der Wegen and Roelvink (2008) and van der Wegen et al. (2008) an MF of 400, whereas Edmonds and Slingerland (2010) used an MF of 175. In the present model, an MF of 365 was chosen for saving simulation time.

3.2. Model setting

As outlined above, a physics-based 2DH longterm morphological numerical model with simplified setting was chosen for the present study. The philosophy is that, given that only principal characteristics of the QE are adopted and key processes of sediment transport are involved, the model is kept as simple as possible. Although certain details cannot be reproduced for comparison with real world observations, the aim is to catch the first-order dynamics of large sand bar formation. The simplified model setting also allows the modeling results to be used in a more universal sense by providing a generalized understanding of estuarine morphology, instead of being limited to the special case of the QE only. In addition, with the help of the simplified setting, it is relatively convenient to study the contributions of different factors, including estuarine convergence, sediment grain size and river discharge, which can then be compared with some other large estuaries. Furthermore, the simple setting meets the requirement of saving computational time for longterm morphological modeling.

The simplest model would be one-dimensional in the longitudinal direction, reasonable features of estuarine morphology having been obtained by 1D numerical modeling approaches in which river discharges were excluded (Lanzoni and Seminara, 2002; Hibma et al., 2003b; Todeschini et al., 2008). However, if river discharge at the landward end of the estuary is involved, our own numerical experiments show that continuously supplied river-borne sediment cannot escape seaward with the result that continuous accumulation occurs in the low-energy transition zone between the river-dominated and the tide-dominated region. This continuous accumulation cannot approach final equilibrium state in a long period (e.g. 6000 year), and creates an unrealistically high sand bar ($\gg$10 m) that indicates the failure of the 1D model. For this reason a 2DH model was employed in this study. Adding the lateral dimension provides the opportunity of the river-borne sediment to be exported via channels fringed by shallow shoals or tidal flats, and which are commonly dominated by ebb tidal currents (Friedrichs and Aubrey, 1988).

Tide-dominated estuaries are usually characterized by a funnel-shaped geometry in plain view, the width of the estuarine section decreasing rapidly landward at an exponential rate (Wells, 1995). The QE is not an exception in this respect. Fig. 3a shows that the estuarine width at any particular point is well described by the following exponential equation:

$$W = \begin{cases} 120\exp\dfrac{x-225}{40} & x \geq 25 \\ 0.8 & x < 25 \end{cases} \quad (1)$$

where W is the estuarine width in km, and x is the distance from the upper tidal limit in km. The numerator of 40 km in Eq. (1) is called the convergence length and is a measure of the estuarine convergence rate, which means that the width is reduced by a factor of e (natural logarithm) for every 40 km in the landward direction (Lanzoni and Seminara, 2002). Therefore, the larger the convergence length is, the smaller the convergence rate becomes. The part landward of 25 km is mostly a fluvial channel with a constant width of 0.8 km. Consequently, For the purpose of investigating the influence of estuarine convergence in general, this schematized plan shape can easily be modified by changing the convergence length.

The modeling geometry was schematized by Eq. (1) in order to resemble the QE (Fig. 5a). The 225 km long longitudinal axis has 150 cells, each having a uniform length of 1.5 km. In the lateral direction, the grid is uniformly discretized into 6 aliquots, i.e. the width of each equals 1/6 of the total width of the estuary, increasing from the land to the sea. The high resolution of the longitudinal grid allows a detailed study of the large sand bar dynamics, which is the focus of the present contribution. The lower resolution of the lateral grid reduces the grid number and hence saves computational time. Because

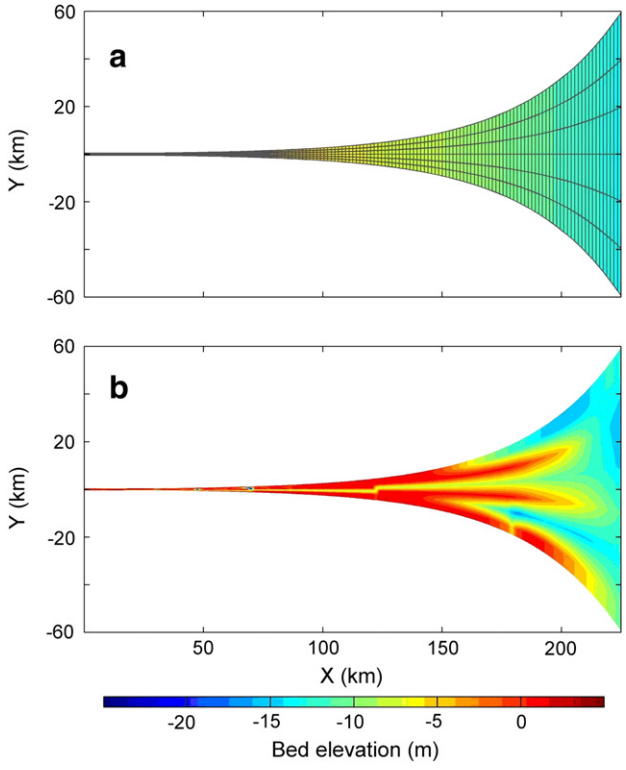

Fig. 5. (a) Modeling grid and initial bathymetry of the schematized Qiangtang estuary in the reference case R; (b) final bathymetry after a 6000 year simulation. Color bar denotes the bed elevation relative to mean sea level (m).

lateral morphological patterns cannot be described by the limited lateral grid, the study concentrates on the longitudinal profile. To fulfill the stability requirement, a numerical calculating time step of 4 min is prescribed.

Initially, a laterally uniform and longitudinally inclined bed with a constant slope of 0.6×10^{-4} was set from the land boundary to the seaward mouth, the elevation decreasing from 0 m above mean sea level (asl) at $x=0$ km to −13.5 m asl at $x=225$ km, according to the present bathymetry at the upper fluvial channel and at the QE mouth, respectively. This initial bathymetry is based on the consideration that this study aimed at elucidating the formation of the large sand bar from a constant slope, and not to reconstruct the infilling history of the estuary. It is for this reason that the ancient bathymetry of the QE was not adopted.

A single sediment grain size of 64 μm was uniformly distributed in the model domain and forms the smallest cohesionless grain size implemented in the Delft3D software. Although 64 μm is coarser than the observed median grain size of 20 to 40 μm in the QE, it was an obvious choice for two reasons. First, the fundamental dynamic property of the cohesionless sediment in the QE could be preserved if a larger natural uniform grain size was chosen. Second, the prediction of cohesive sediment transport is more complex and highly sensitive to the input parameters such as the erosion constant, the critical erosion and deposition bed shear stresses, and the sediment bulk density (Whitehouse et al., 2000). Furthermore, due to the lack of field calibration of these parameters, a variety of results could be achieved by changing them artificially.

The land and sea boundaries were forced by tidal and river discharge. At the open sea boundary, only the main M2 tide was taken into account for simplification (Todeschini et al., 2008; van der Wegen and Roelvink, 2008; van der Wegen et al., 2008). According to the observations and the hydrodynamic modeling results of the QE by Xie et al. (2009), a uniform tidal range of 2.5 m across the whole mouth (the open sea boundary) was chosen in order to resemble the real situation. The inland open boundary was defined by a constant river discharge of 1000 $m^3\,s^{-1}$, which is in accordance with the hydrography of the Qiangtangjiang River. The lateral boundaries were closed. At the open boundaries of the sea and the inland, dynamic equilibrium concentrations were defined for sediment transport (Hibma et al., 2003b). This definition determines the sediment concentration in the water column at the open boundaries by the local pickup and deposition terms. The relatively shallow water depth at the seaward boundary (13.5 m) and the definition of equilibrium concentrations implied an abundant sediment availability to be imported through the mouth, which is consistent with the condition of sufficient sediment supply from the Changjiang River into the QE.

Because the large sand bar has a temporal formation scale of the order of 10^3 years (Chen et al., 1964), the model was simulated for 6000 years to make sure that the system was able to reached equilibrium.

3.3. Sensitivity analysis

A sensitivity analysis was carried out to evaluate the effects of estuarine convergence, sediment grain size, and river discharge on the longitudinal profile, which may improve the understanding of the generalized estuarine morphological model. In addition, some of the results of the sensitivity analysis would be suitable to be compared with other large tide-dominated estuaries because they share similar key forcing factors. The settings of the sensitivity analysis are summarized in Table 1.

At first, the estuarine convergence rate was modified. Based on Eq. (1), which represents the geometry of the reference case (case R), the case S was designed with a slower convergence rate using the following equation:

$$W = 120\exp\frac{x-225}{50} \tag{2}$$

Table 1
Settings for the sensitivity analysis. Case R is the reference case.

No.	Convergence length (km)	Sediment	River discharge (m^3/s)
Case R	40	One fraction of 64 μm	1000
Case S	50	One fraction of 64 μm	1000
Case G	40	3 fractions of 2000, 500, 125 μm	1000
Case R1	40	One fraction of 64 μm	0
Case R2	40	One fraction of 64 μm	250
Case R3	40	One fraction of 64 μm	2000

As can be seen, the convergence length was modified from 40 km in Eq. (1) to 50 km in Eq. (2), but the estuarine mouth width of 120 km was kept the same. One of the considerations to choose this design was that, due to the completed and still planned land reclamations during the past several decades and in the future, respectively, the geometry of the QE tends to be changed, causing a stronger degree of convergence. This sensitivity analysis is therefore useful to evaluate the impacts of these construction activities on the estuarine morphology.

In a second step, the influence of sediment grain size was investigated. As outlined above, the QE is fed by a sufficient amount of fine cohesionless sediment both from the river and from the Changjiang Estuary through the estuary mouth, whereas the Bristol Channel–Severn Estuary and the Cobequid Bay–Salmon River Estuary are characterized by limited fine sediment supply. This contrast should result in a significant difference in the morphology. Here the Cobequid Bay–Salmon River Estuary was taken as the prototype for the sensitivity analysis in the case G employing three typical grain sizes, namely −1 phi (2000 μm), 1 phi (500 μm), and 3 phi (125 μm) representing a gravel/very coarse sand, a coarse/medium sand, and a fine/very fine sand fraction, respectively. Initially, the three fractions were equally weighted and well-mixed in the stratigraphy with a uniform distribution over the entire model domain. The multi-sized sediment transport model was then used to simulate the co-evolution of the morphology and the grain-size distribution. In the supplemental material, more systematical sensitivity analysis on the sediment grain size is demonstrated.

The third series of sensitivity analysis was on the river discharge effect. The discharge of 1000 $m^3\,s^{-1}$ in the reference case R matches the situation of the QE but is substantially lower in the case of some other large tide-dominated estuaries. For example, the River Severn has an average annual discharge of 107 $m^3\,s^{-1}$ (Centre for Ecology and Hydrology, Natural Environment Research Council, UK), that of the Salmon River is approximately 10 $m^3\,s^{-1}$ (Dalrymple et al., 1990), while the Gulf of Kachchh, India, lies in a semi-arid region with small river discharge (Chauhan et al., 2006). In accordance, three test cases were designed with river discharges of 0, 250, and 2000 $m^3\,s^{-1}$, respectively. It is noted that, because of the equilibrium concentrations for sediment transport at the boundary, the increasing river discharge are associated with the increase of river sediment supply. Therefore, this series of sensitivity analysis is related to both water and sediment supply from rivers.

In addition to the above three series, sensitivity analyses on the tidal ranges and the model parameters in sediment transport calculation (the bed slope effect and the different sediment transport formulations) were carried out and shown in the supplemental material.

4. Results

4.1. Reference case R

The bathymetric map of the whole domain of reference case R after a 6000-year modeling period is illustrated in Fig. 5b. Although the lateral patterns are excluded from the present study because of the limited number of lateral cells, it is noted that the final bathymetric map

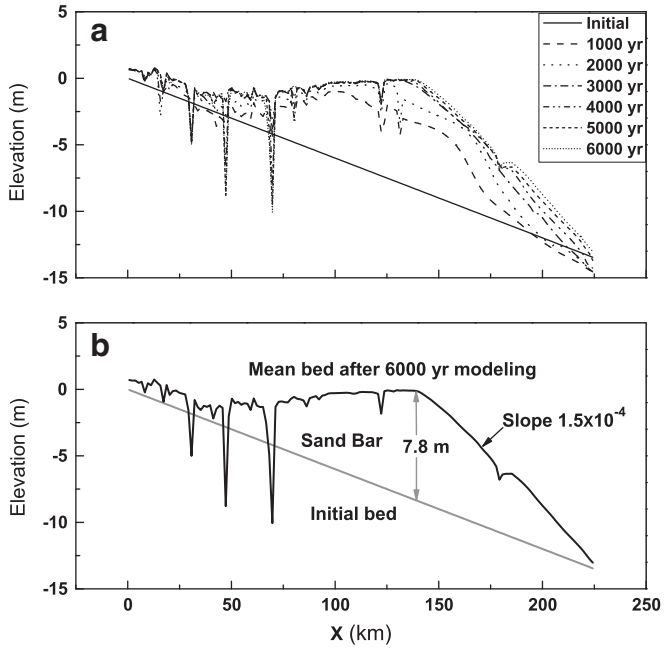

Fig. 6. (a) Longterm evolution of the longitudinal bed profile of the case R; (b) the final (6000 years) equilibrium mean longitudinal bed profile outlining the large sand bar.

indicates the formation of channels through which river water and sediment can be exported once the final morphological equilibrium is achieved.

The longterm evolution of the averaged longitudinal bed profile in the case R is shown in Fig. 6a. It can be seen that sediment accumulates in the middle part of the estuary and that the basic feature of the large sand bar emerges after 1000 years. It then continues to gradually grow until, after 3000 years, the shape of the sand bar approaches a stable form, suggesting that the equilibrium configuration is reached asymptotically. Compared to the 1000 year situation, the height of the bar only increased by about 1 m, but the position of the maximum height moved seaward from $x=100$ km to $x=130$ km, the final profile having a relatively flat top between these two positions. On the equilibrium bed profile, the large sand bar can be identified between $x=50$ km and the estuary mouth, having a front slope of 1.5×10^{-4} and a peak crest height of 7.8 m above the initial bed level (Fig. 6b).

In Fig. 7, the hydrodynamics at the final equilibrium state are evaluated. First, the tidal phase is delayed by 1 to 1.5 hour every 45 km from the estuary mouth toward the land. Second, the velocity amplitude increases between $x=180$ and $x=135$ km, and then declines landward, indicating a hypersynchronic condition. Third, tidally induced currents dominate most of the estuary, as indicated by similar maximum flood and ebb current speeds, except that at $x=45$ km the seaward current is substantially intensified, which suggests a contribution from river discharge. Fourth, because of bed friction the incoming temporally symmetrical tide is modified, the flood phase having a shorter period than the ebb phase.

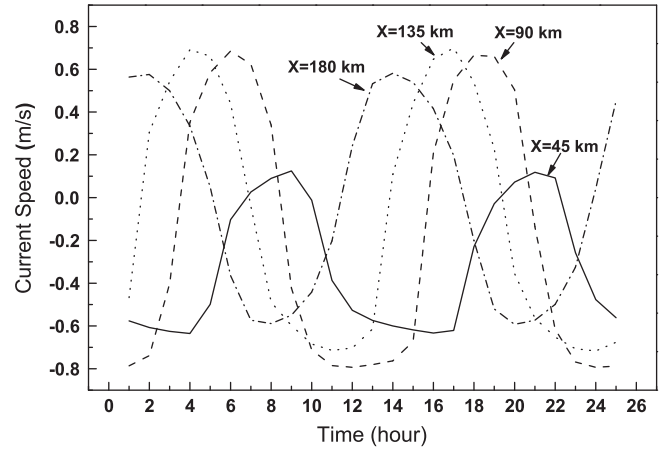

Fig. 7. Time series of the current velocities in the case R at the final state, positive values denoting the flood, negative values the ebb current.

The longitudinal hydrodynamic and sediment transport situations at the initial and final states of case R are illustrated in Figs. 8, and 9, respectively. At the initial state, the longitudinal profile of tidal ranges shows the typical hypersynchronic character (Fig. 8a). The maximum flood speed is higher than the maximum ebb speed from $x=225$ to $x=50$ km, the difference increasing from the mouth. When approaching $x=45$ km, this difference decreases to zero and then, along with the rapidly decreasing maximum flood speed, the system is overturned and now has a higher maximum ebb speed (Fig. 8b). In Fig. 8c, the intensity of river discharge is locally represented by the absolute value of the residual velocity, the tidal current speed being represented by half of the difference of the maximum (positive) and minimum (negative) current velocity, the total energy being estimated by the maximum current speed. It can be seen that, associated with the landward increase in river and decrease in tidal contribution, the total energy is initially enhanced from the mouth

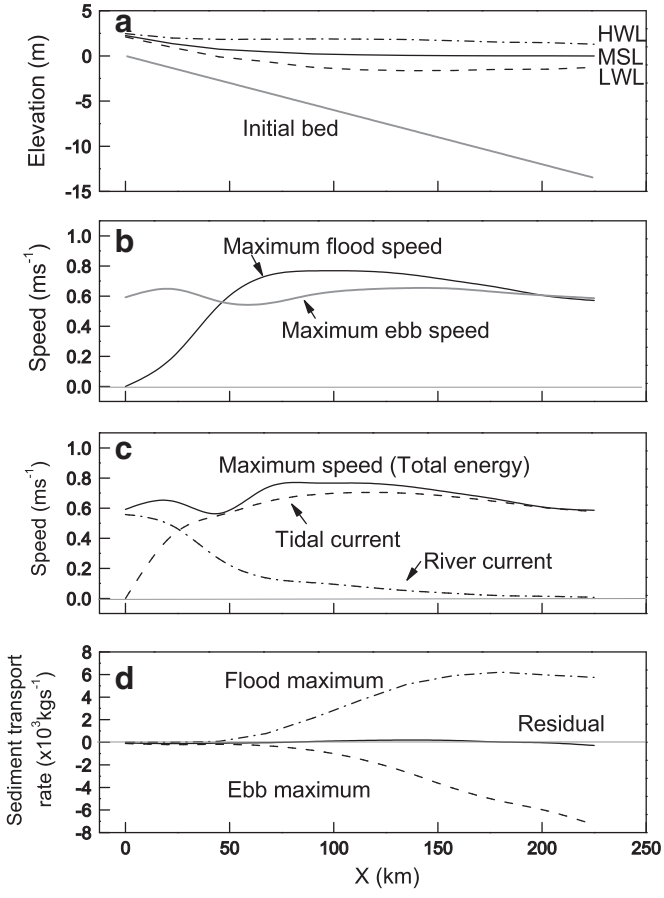

Fig. 8. The longitudinal distribution of hydrodynamics and sediment transport at the initial state of case R. (a) The high-water level (HWL), mean sea level (MSL) and low-water level (LWL). (b) Maximum current speeds during flood and ebb tides. (c) Intensity of the river current as represented by the absolute values of the residual velocity, the tidal current being represented by the half values of the difference between the maximum (positive) and minimum (negative) current velocities, and the total energy being defined by the maximum current speeds. (d) The maximum cross-sectional sediment transport rates during flood and ebb tides, and the residual sediment transport rates.

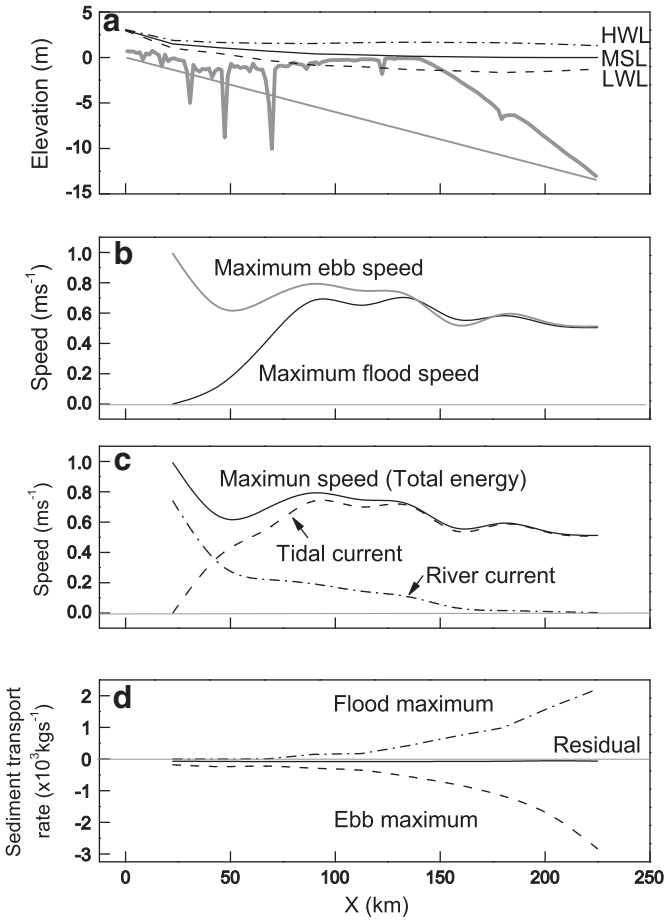

Fig. 9. Longitudinal distribution of hydrodynamics and sediment transport at the final equilibrium state of case R illustrated by the same panels as in Fig. 8.

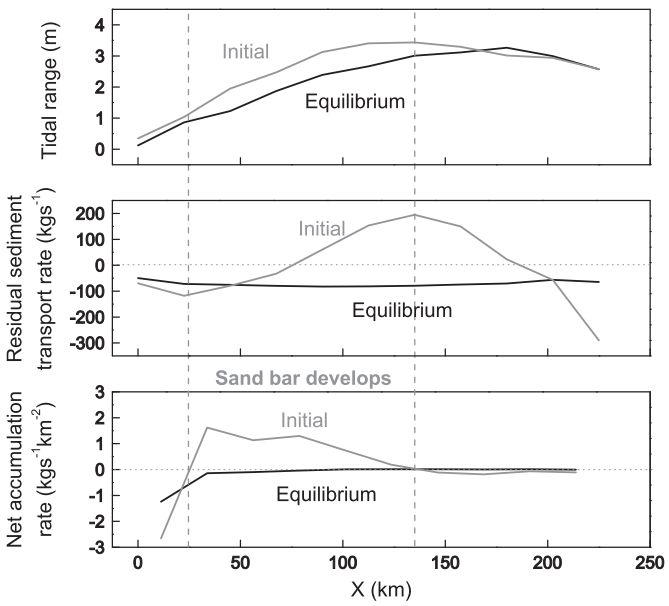

Fig. 10. Comparison between the initial and the final equilibrium states of case R: the longitudinal distributions of tidal range, cross-sectional residual sediment transport rate, and net accumulation rate, positive values denoting the flood direction or the net deposition, and negative values denoting the ebb direction or the net erosion. The net deposition area is located where the sand bar initially develops.

landward due to the increase in the dominant tidal current, but then reaches a trough at a location close to the turning point between the dominance of the maximum flood and ebb speeds shown in Fig. 8b. The maximum cross-sectional sediment transport rates during the flood and ebb tides are shown in Fig. 8d, indicating that, in the middle part of the estuary, sediment transport is significantly higher during the flood phase as compared to the ebb phase. As a consequence, the estuary has a large accommodation space, allowing sediment supplied from both the river and the sea to accumulate.

The longitudinal variations of the same parameters at the final equilibrium state of the morphological evolution are illustrated in Fig. 9. The maximum ebb speed now exceeding the maximum flood speed over most of the estuary, and the longitudinal patterns of river current, tidal current and total energy are almost the same as during the initial state, except that the peaks of the curves have shifted. The enhanced ebb current in Fig. 9b is responsible for the amplified ebb sediment transport shown in Fig. 9d. As a consequence, excess sediment supplied by the river can now be exported, causing net sediment accumulation to approach zero as morphological equilibrium is reached. The estuary is thus gradually transformed from a sink for sediment derived from both land and sea to a transit area that is bypassed by sediment supplied from the river, while sediment formerly entering the estuary from the seaward side is blocked because the accommodation space has disappeared. In this respect, the estuarine system is similar to the graded river concept, which describes the long-term equilibrium state of a river system subject to steady allogenic forcing (Mackin, 1948).

In Fig. 10, the initial and final states concerning the tidal range, cross-sectional residual sediment transport rate, and net accumulation for case R are compared. Because the evolution of the large sand bar induces a progressively stronger bottom friction, the initial state has an overall higher tidal range. The turning point where the initial increase in tidal range (hypersynchronic mode) reverses to a decreasing range (hyposynchronic mode), has shifted seaward in spite of the fact that the maximum tidal ranges are almost the same. At the initial state, sediment is on average transported landward in the middle part of the estuary, but seaward in both the upper part and at the estuary mouth. The convergence of sediment transport caused by net seaward transport in the upper estuary and net landward transport in the middle estuary produces net accumulation between the two areas as a result of which the large bar is formed. Fig. 10 shows that the net depositional area, and hence the location of incipient bar formation, is situated between $x = 25$ and $x = 135$ km. At the final state, the whole estuary has a nearly constant seaward transport rate for sediment supplied by the river, which results in an almost zero accumulation rate as required by the equilibrium state.

4.2. Sensitivity analysis

The influence of the estuarine convergence rate is demonstrated in Fig. 11, implying that strong convergence causes the sand bar to grow in the seaward direction. The landward parts of the profiles are almost the same in both cases, whereas the head of the sand bar in case S is located around 20 km further landward. The crest has an elevation close to that of case R, but its position has shifted landward from $x = 130$ to $x = 90$ km. These results suggest that a 10 km increase in convergence length from case R to case S causes a pronounced retreat of the sand bar head and crest. This sensitive response can be attributed to the stronger flood dominated tidal force induced by the stronger convergence, which pushes more sediment into the estuary to form the larger sand bar (Friedrichs and Aubrey, 1994).

The effect of sediment grain size on the estuarine morphology is evaluated and illustrated. In Fig. 11c it can be seen how the initially mixed sediment (1 phi) has become size-sorted longitudinally along the bar after 6000 years. The finest sediment is pushed downstream by river currents in the upper area and upstream by flood-

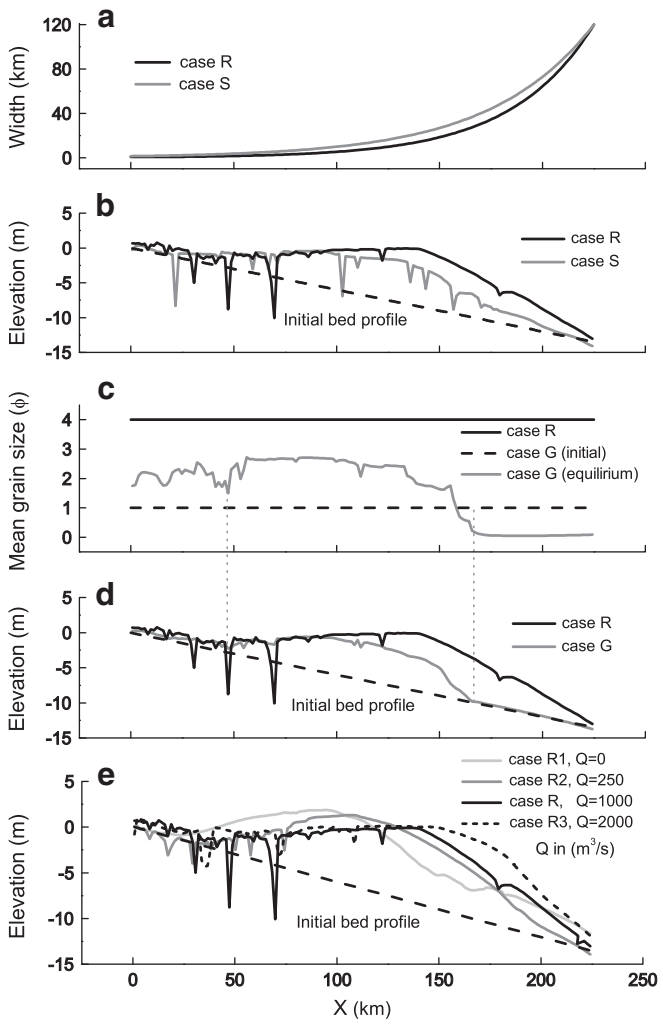

Fig. 11. Sensitivity analysis. The effect of estuarine convergence (case S): (a) longitudinal distribution of estuarine widths; (b) longitudinal bed profiles after the 6000 year modeling period. The effect of sediment grain size (case G): (c) longitudinal distribution of mean grain sizes; (d) longitudinal bed profiles after the 6000 year modeling period; (e) the effect of river discharge (cases R1, R2, and R3) on the longitudinal bed profiles after the 6000 year modeling period. Case R is the reference case (see Table 1 for details).

dominated currents in the mouth area, and the sediment then accumulating around the point of sediment convergence, as a result of which the bar in the middle estuary is associated with the finer sediment. At the seaward end, bed armoring has taken place because of the winnowed fine fraction from the top layer. The armored bed has a mean size of 0 phi (1000 μm), being coarser than the largest grains that the currents can move. Due to the equilibrium sediment concentration at the boundary, the armored bed prevents further sediment import from the open sea, resulting in a starved sediment supply condition here. As a consequence, the lack of sediment produces a sand bar of reduced size (Fig. 11d). Compared with case R, the bar head is located 25 to 40 km further landward in case G, although the elevation of the bar crest is almost the same.

The results of the three test cases used to investigate the effect of river discharge are illustrated in Fig. 11e. A twofold response of the longitudinal bed profiles to changing river discharge is observed. First, the bar head shifts seaward with increasing discharge. Second, with the exception of case R3 representing the largest discharge, lower discharge is associated with a higher elevation of the bar crest. It can also be seen that the crest elevations of case R1 and case R2 are above the mean sea level. Low discharge systems thus tend to have shorter but higher sand bars. This can be interpreted to show that enhanced river currents cause an increase in river sediment supply and stronger downstream sediment transport, thereby flattening the bar and promoting seaward bar progradation.

5. Discussion

5.1. Comparison with the Qiangtangjiang Estuary

Comparing the modeling results with the modern QE reveals that the equilibrium large sand bar is successfully simulated by the numerical modeling, and that the shape, size and position of the modeled bar are reasonably similar to that of the modern QE, as can be seen by comparing Figs. 3, and 6. Both bars have the same front slope of 1.5×10^{-4}. The modeled bar begins at a position in the upper estuary close to that of the observed one, but it extends 50 km further toward the mouth, resulting in a bar body having a total length of 175 km. The crest height of the modeled bar is 7.8 m above the initial bed compared with 10.4 m of the modern bar. The modeled bar has a flat top with the crest located further seaward in accordance with the larger bar body. Although there are some inconsistencies in detail, the overall similarity with the modern bar suggests that the schematized numerical model is able to reproduce the first-order characteristics of the large sand bar in the QE.

The lack of detailed information on the temporal evolution of the QE makes it currently impossible to fully verify the modeling results. The model predicts that the basic feature of the large sand bar evolves within 1000 years, which is consistent with the time period available for bar formation after the establishment of the funnel-shaped geometry of the QE (Chen et al., 1964). The seaward displacement of the bar crest (Chen et al., 1964) is also predicted by the numerical modeling approach. Finally, the equilibrium bed profiles were obtained after about 3000 years in both the observations and the modeling (Chien et al., 1964).

The net accumulation in the QE over the past several decades can be interpreted to be the result of estuarine geometry modifications induced by land reclamation activities. The sensitivity analysis shows that the growth of the sand bar is positively correlated with the degree of estuarine convergence (see Fig. 11b). The intensified land reclamation, especially in the upper part of the estuary, has resulted in stronger convergence (Han et al., 2003) and hence in renewed net accumulation and sand bar growth.

The differences between the observed and the modeled sand bar mainly concern the seaward extension of the bar head, a feature that can be explained by the simplified model settings. In terms of the sensitivity analysis, a reduced estuarine convergence rate should cause a pronounced retreat of the bar head (see Fig. 11b). Fig. 3a shows that, in the mouth area, the measured longitudinal width has a much slower convergence rate than the schematized curve. Compared with the observed bed profile, the schematized modeling domain evidently allows the bar to become larger and to extend further seaward.

Another possible reason for the difference may be the presence of waves in the mouth region. Waves from the open sea will penetrate some distance into the estuary, although bed friction in shallow water will then rapidly dissipate the wave energy. The wide estuary mouth favors the initial growth of local wind waves. As a result, although tidal currents play the predominant role in sediment transport, wave action cannot be entirely ignored in the mouth area (Dalrymple and Choi, 2007). For example, the importance of swell waves was documented by Harris et al. (2004) in affecting sediment dispersal at distributary channel mouths. Observed waves are on average 0.5 m high in the mouth and these may well interact with the tidal currents to prevent the seaward growth of the modern sand bar. In addition, the QE on average suffers three typhoon invasions every year (Guo et al., 2009). The associated strong wave activity may therefore induce intensive seabed erosion in the mouth area.

Because the simplified model does not involve wave processes, the modeled bar has a greater potential for seaward growth than the observed one.

5.2. Comparison with other numerical modeling results and other large funnel-shaped tide-dominated estuaries

The model case R1 can be compared with the 1D numerical model of Todeschini et al. (2008) (Fig. 12) because both have assumed zero river discharge. The modeled bed profiles in the two approaches show a high degree of similarity, in spite of the differences in the model dimensions and the initial bed profiles. Both sand bars have a crest elevation above the mean sea level and a concave-up front profile. Also the influence of convergence is identical in the two approaches, the strong degree of convergence producing a seaward extension of the large sand bars.

Three other large estuaries have been selected for comparison with the QE and the modeling results: the Cobequid Bay–Salmon River Estuary, Bay of Fundy, Canada, the Bristol Channel–Severn Estuary, UK, and the Gulf of Kachchh, India (Fig. 14). All three share the same characteristics with the QE in that the domain is large (the length scale of 10^2 km), funnel-shaped, and tide-dominated.

The Cobequid Bay–Salmon River Estuary is located at the head of the eastern arm of the Bay of Fundy (Fig. 13a) and is associated with a limited river input (annual average discharge being approximately 10 $m^3 s^{-1}$). It consists of four morphological zones between the seaward and landward tidal limits: zone 0 — the non-depositional subtidal floor of the Minas Basin and outer Cobequid Bay; zone 1 — tidal sand-bar complex; zone 2 — upper-flow-regime sand flats; and zone 3 — the tidally influenced fluvial channel (Dalrymple et al., 1990). The spatial grain-size distribution is illustrated in Figs. 13a, and 14. The outer part of the estuary is occupied by an armoring layer of coarse lag deposits that protect the underlying finer sediment from erosion, the winnowed material having been transported into the estuary to form the sand-bar complex and sand flats (Amos, 1978; Dalrymple et al., 1990). The estuary has a seaward-fining trend in the inner fluvial-dominated part, and a landward-fining trend in the seaward part as a result of which the finest grain sizes are found on the sand-bar complex and sand flats (Fig. 14).

Compared with the QE, the Cobequid Bay–Salmon River Estuary differs in two respects. First, the sand bar and sand flats are located more landward. Second, the longitudinal coarse-fine-coarse trend of the surficial sediments and the armoring layer in the outer estuary. Both of them can be qualitatively interpreted by the results of the sensitivity analysis. The effect of river discharge illustrated in Fig. 11e shows that low river input causes a landward displacement of the large sand bar, while the limited sediment supply in case G leads to a retreat of the bar head (Fig. 11d). The low river discharge (10 $m^3 s^{-1}$) and the limited sediment supply, which is associated with armoring in the outer part, prevent a seaward growth of the sand bar and sand flats. The spatial grain-size variations are due to the tidal sorting processes. The landward net transport winnows fine grains from the active surface layer, leaving behind the armoring lag deposits, the fine sediment accumulating in the upper part of the estuary to form the bulge in the longitudinal bed profile. The sensitivity analysis on the effect of sediment supply clearly reveals the importance of these processes, and the modeled grain-size profile of case G in Fig. 11c reasonably resembles the observed coarse-fine-coarse trend in Fig. 14.

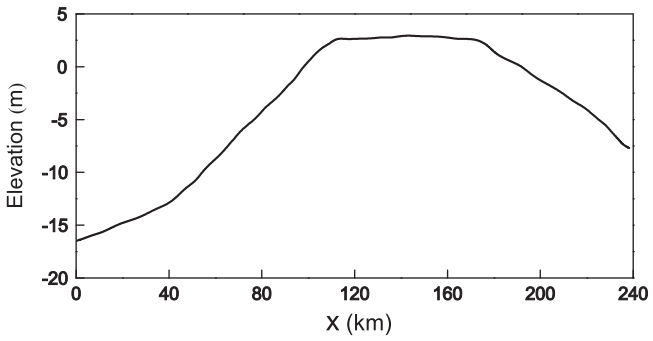

Fig. 12. The equilibrium longitudinal bed profile of the 1D modeling result. Modified from Todeschini et al., 2008.

The Bristol Channel–Severn Estuary is the largest estuary on the west coast of England (Fig. 13b). The main part of the Bristol Channel is scoured clear of bed sediments to expose the underlying bedrock or is covered by lag gravels (Harris, 1988). Sandy and muddy materials are deposited in the Severn Estuary and at the heads of smaller bays in the Bristol Channel, including Swansea Bay and Bridgewater Bay. Although the Severn is the longest river in Britain, its annual average discharge is only 107 $m^3 s^{-1}$, being less than that of the Qiangtangjiang River by one order of magnitude. Allen (1991) suggested that the sand in the Severn Estuary originated from the Bristol Channel, and that the mud has a fluvial source. The sand accumulation in the Severn Estuary and sediment starvation in the Bristol Channel can be explained by the same reasoning as in the case of the Cobequid Bay–Salmon River Estuary: namely the combined effects of river discharge and sediment supply.

The Gulf of Kachchh, in turn, is a large coastal embayment along the northwest coast of India (Fig. 13c). Because of the semi-arid climate, river discharge is very small. The Indus River, one of the major rivers of the world, is located about 150 km to the northwest. The bathymetric map shows that, in the head part of the bay, the distance between the 20 m and 10 m contours is smaller than that between the 10 m and 5 m contours, implying a bar-shaped bulge in the longitudinal bed profile. Muddy sediments occur in a tie adjacent to the northern coastline and the bay head, the most probable source being the Indus River (Chauhan et al., 2006; Ramaswamy et al., 2007). The central and the southern parts of the bay are covered by sand or exposed bedrock, and a rough sequence of rock–sand–mud can be identified towards the bay head. Contrary to the Changjiang Estuary located close to the QE, the remote source of the Indus River cannot provide sufficient sediment to form a large bar at the head and in the central part of the Gulf of Kachchh because of the relatively large distance between the bay and the Indus River. The small local river discharge, in turn, causes the bar to be located further headward in the Gulf of Kachchh, as intimated by the bathymetry in Fig. 11e.

5.3. The unique position of the Qiangtangjiang Estuary within the general framework of estuarine morphology

In general, bottom friction induces flood-dominated tidal currents, causing a net landward sediment transport. In the upper parts of estuaries, river discharge pushes sediment seaward due to small channel cross-sectional areas and tidal prisms. The two converging transport processes meet at some point in the middle estuary, creating a bar along the longitudinal bed profile as a consequence. The new morphology then causes feedbacks to the hydrodynamics, which lead to a progressive decrease in tidal distortion (Lanzoni and Seminara, 2002). As a result, the point of sediment transport convergence gradually moves in the seaward direction. Eventually, the sediment supplied by the river begins to bypass the estuary and further import of sediment from the adjacent sea is blocked. Once net deposition and erosion are balanced, an equilibrium bed profile is established. Previous numerical modeling studies have established equilibrium morphological configurations without the contribution of water and sediment from the river (Lanzoni and Seminara, 2002; Hibma et al., 2003b; Todeschini et al., 2008). The present results indicate that estuaries are not always transient geomorphological features but that, in some cases, longterm interactions between fluvial

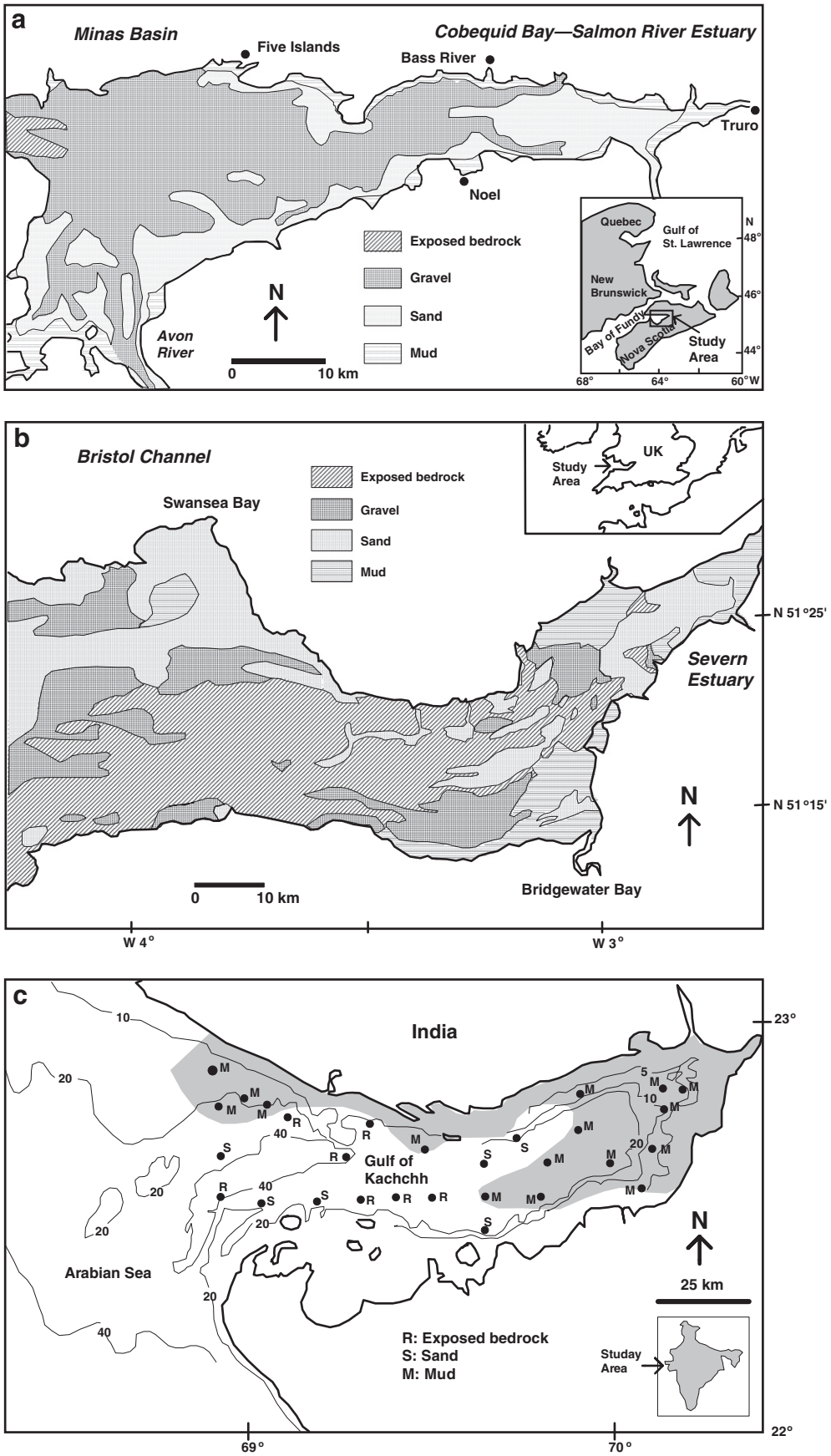

Fig. 13. (a) Distribution of surficial sediment types in the Cobequid Bay–Salmon River Estuary, Bay of Fundy, Canada. (b) Distribution of surficial sediment types in the Bristol Channel–Severn Estuary, UK. (c) Distribution of surficial sediment types and bathymetry in the Gulf of Kachchh, India, the mud bed being highlighted by shadowing.
Panel (a) is modified after Dalrymple et al., 1990; panel (b) is modified after Harris, 1988; and panel (c) is modified after Kunte et al., 2005; Ramaswamy et al., 2007.

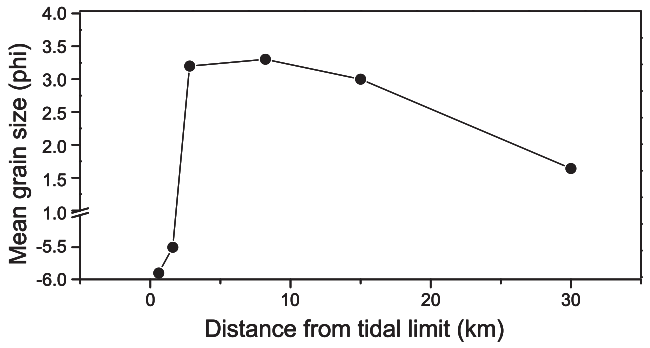

Fig. 14. The longitudinal mean grain-size distribution in the Cobequid Bay–Salmon River Estuary, Bay of Fundy, Canada.
Modified from Dalrymple and Choi, 2007.

and marine processes can keep an estuary in an equilibrium state, preventing it from being infilled by river-borne sediment to evolve into a delta.

The bars scale with the different forcing factors in the estuaries. The sensitivity analysis and the comparison with other estuaries demonstrate the importance of estuarine convergence, sediment supply and river discharge. Strong convergence causes the growth of the bars by seaward extension, while coarser sediments and reduced sediment supply cause the bar head to retreat landward, restricting it to the upper section of the estuary. While the position of the bar head extends seaward under large river discharge, the elevation of the bar crest is negatively correlated with river discharge. In this context, the QE is a unique example. The strong degree of the convergence, which can be measured by the convergence length of 40 km, a sufficient cohesionless fine sediment supply from the adjacent Changjiang River, and a river discharge of around 1000 $m^3 s^{-1}$, have shaped a large sand bar with a total length of 125 km and a crest height of 10 m above the estuarine baseline.

In the generalized morphological model of tide-dominated estuaries recently suggested by Dalrymple and Choi (2007) (Fig. 15), the schematic estuarine geometry is characterized by a funnel shape, elongate tidal sand bars in the seaward section, fringing muddy tidal flats and salt marshes, and straight-meandering-straight transitions in the channel pattern. It is important to note here that the elongate tidal bars (also called tidal ridges) representing a series of bedforms identified in estuarine cross-sections are fundamentally different from the large bar of the present study, which merely forms a pronounced bulge in the longitudinal bed profile. In fact, the elongate tidal bar area in the model of Dalrymple and Choi (2007) would be the front part of the large sand bar.

In spite of apparent differences, the fundamental morphological and hydrodynamic characteristics of the Dalrymple and Choi (2007) model are nevertheless comparable to the numerical modeling results presented here. The limited number of lateral grid cells prevents the development of lateral channel-ridge patterns in the model, although the estuarine bathymetry in Fig. 5b does show some reasonable similarity with the schematic morphological map in Fig. 15. The longitudinal distribution of river and tidal currents, and the high-low-high-low trend of the total energy in Fig. 15 are consistent with the numerical results in Figs. 8, and 9, even though waves were not involved in the present numerical modeling study.

Comparing the QE morphology with the Dalrymple and Choi (2007) model, most of the features are similar, including the tidal sand ridge system and the fringing muddy tidal flats (Fig. 2), only the straight-meandering-straight transitions of the channel pattern being an exception. Instead of the meandering channel, the fluvial to marine transition zone of the QE is characterized by a laterally migrating channel thalweg. This difference can be explained by the cohesionless character of the sediment in the QE. Sustainable channel meandering needs some form of bank stabilization (Chien, 1985). In this context, experimental studies have shown that the strength of the elevated bank, which can be provided by cohesive sediment and/or vegetation, is crucial for the development of meandering channels (Schumm and Khan, 1972; Peakall et al., 2007; Braudrick et al., 2009; Tal and Paola, 2010). The lack of cohesive sediment and vegetation in the QE thus prevents the development of a meandering channel and, instead, favors the formation of the lateral channel migration pattern (Chien, 1985).

6. Conclusion

It has been demonstrated that the evolution and the development of an equilibrium state of the large sand bar in the QE can be simulated by a 2DH numerical modeling approach. The basic feature of the large sand bar is predicted to appear 1000 years after formation of

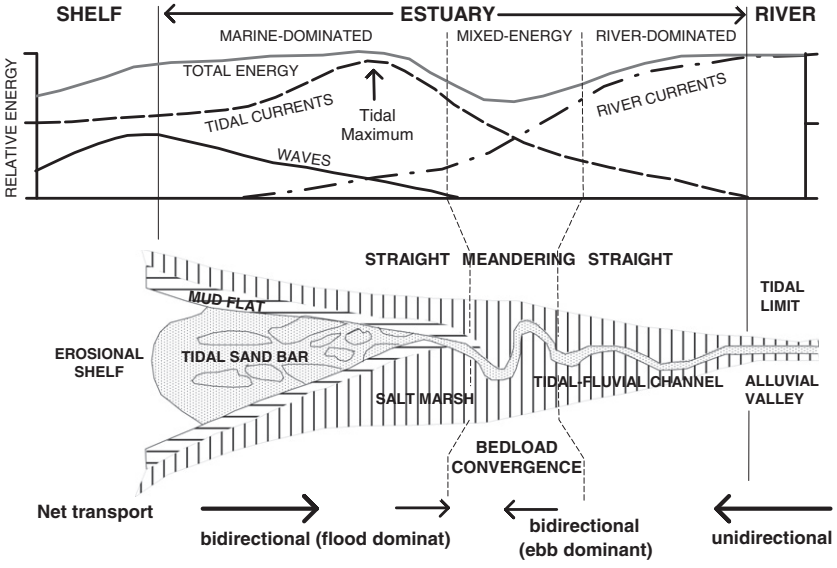

Fig. 15. Schematic geomorphological map of a tide-dominated estuary and the longitudinal variations in the intensity of the three main physical processes of river currents, tidal currents and wave action. The resulting directions of net bedload sediment transport are indicated by the arrows at the bottom.
After Dalrymple and Choi, 2007.

the modern estuarine plan geometry in the middle estuary where the net landward sediment transport caused by the flood-dominated tide meets the net seaward sediment transport induced by the prevailing river discharge. Feedbacks of the newly developing morphology to the hydrodynamics then reduce the tidal distortion, which results in a decreasing rate of sediment convergence. The sand bar gradually grows until 2000 years later the net seaward transport occupies the whole estuary and the river supplied sediment bypasses the estuary to the sea. From this time onward, the bar morphology gradually approaches an equilibrium state.

It has also been demonstrated that three major forcing factors play an important role in estuarine morphology. A strong degree of convergence causes the growth of the bar by seaward extension of the bar head, whereas coarser sediment and a reduced sediment supply cause the bar head to retreat landward, bar development being then restricted to the upper section of the estuary. The position of the bar head also shifts seaward with increasing river discharge, although the elevation of the bar crest is negatively correlated with river discharge. The strong degree of convergence, a sufficient supply of cohesionless fine sediment from the adjacent Changjiang River, and a river discharge of around $1000\ m^3\ s^{-1}$ thus control the shape of the unique large sand bar in the QE.

Acknowledgments

The study was supported by the Senckenberg Institute, the Chinese Scholarship Committee (CSC) and the Natural Science Foundation of China (NSFC, grant numbers 40830853 and 40906042). The constructive comments of two anonymous reviewers have substantially contributed to improving the clarity of the manuscript.

Appendix A. Supplementary data

Supplementary data to this article can be found online at doi:10.1016/j.margeo.2011.12.008.

References

Allen, J.R.L., 1990. The Severn Estuary in southwest Britain: its retreat under marine transgression, and fine-sediment regime. Sediment. Geol. 66, 13–28.
Allen, J.R.L., 1991. Fine sediment and its sources, Severn Estuary and inner Bristol Channel, southwest Britain. Sediment. Geol. 75, 57–65.
Amos, C.L., 1978. The post glacial evolution of the Minas Basin, N.S.: a sedimentological interpretation. J. Sediment. Petrol. 48, 965–982.
Bhattacharya, J.P., 2003. Deltas and estuaries. In: Middleton, G.V. (Ed.), Encyclopedia of Sediments and Sedimentary Rocks. Kluwer, Dordrecht, pp. 195–203.
Braudrick, C.A., Dietrich, W.E., Leverich, G.T., Sklar, L.S., 2009. Experimental evidence for the conditions necessary to sustain meandering in coarse-bedded rivers. Proc. Natl. Acad. Sci. U. S. A. 106, 16,936–16,941.
Chang, T.S., Flemming, B.W., Bartholomä, A., 2007. Distinction between sortable silts and aggregated particles in muddy intertidal sediments of the East Frisian Wadden Sea, southern North Sea. Sediment. Geol. 202, 453–463.
Chauhan, O.S., Jayakumar, S., Menezes, A.A.A., Rajawat, A.S., Nayak, S.R., 2006. Anomalous inland influx of the River Indus, Gulf of Kachchh, India. Mar. Geol. 229, 91–100.
Chen, J., Luo, Z., Chen, D., Xu, H., Qiao, P., 1964. The forming and historical evolvement of the big sand bar inside the Qiantangjiang Estuary. Acta Geog. Sin. 30, 109–123 (in Chinese with Russian abstract).
Chen, Z., Stanley, D.J., 1998. Sea-level rise on Eastern China's Yangtze Delta. J. Coast. Res. 14, 360–366.
Chien, N., 1985. On the classification and causes of formation of different channel patterns. Acta Geog. Sin. 40, 1–10 (in Chinese with English abstract).
Chien, N., Sie, H., Chow, C., Lee, Q., 1964. The fluvial processes of the big sand bar inside the Chien Tang Chiang Estuary. Acta Geog. Sin. 30, 124–142 (in Chinese with English abstract).
Dalrymple, R.W., Baker, E.K., Harris, P.T., Hughes, M., 2003. Sedimentology and stratigraphy of a tide-dominated, foreland–basin delta (Fly River, Papua New Guinea). In: Sidi, F.H., Nummedal, D., Imbert, P., Darman, H., Posamentier, H.W. (Eds.), Tropical Deltas of Southeast Asia—Sedimentology, Stratigraphy, and Petroleum Geology: SEPM Special Publication, 76, pp. 147–173.
Dalrymple, R.W., Choi, K., 2007. Morphologic and facies trends through the fluvial-marine transition in tide-dominated depositional systems: a schematic framework for environmental and sequence-stratigraphic interpretation. Earth Sci. Rev. 81, 135–174.
Dalrymple, R.W., Knight, R.J., Zaitlin, B.A., Middleton, G.V., 1990. Dynamics and facies model of a macrotidal sand-bar complex, Cobequid Bay–Salmon River Estuary (Bay of Fundy). Sedimentology 37, 577–612.
Dalrymple, R.W., Zaitlin, B.A., Boyd, R., 1992. Estuarine facies models: conceptual basis and stratigraphic implications. J. Sediment. Petrol. 62, 1130–1146.
Dastgheib, A., Roelvink, J.A., Wang, Z.B., 2008. Long-term process-based morphological modeling of the Marsdiep Tidal Basin. Mar. Geol. 256, 90–100.
de Swart, H.E., Zimmerman, J.T.F., 2009. Morphodynamics of Tidal Inlet Systems. Annu. Rev. Fluid Mech. 41, 203–229.
Dronkers, J., 2005. Dynamics of coastal systems. Advanced Series on Ocean Engineering, vol. 25. World Scientific, Singapore. 520 pp.
Dyer, K.R., 1986. Coastal and Estuarine Sediment Dynamics. John Wiley and Sons, Chichester. 342p.
Dyer, K.R., 1997. Estuaries–Physical Introduction, 2nd ed. John Wiley and Sons, Chichester. 195 pp.
ECCHE (Editorial Committee for Chinese Harbors and Embayments), 1992. Chinese Harbours and Embayments (Part V). China Ocean Press, Beijing. 357 pp (in Chinese).
ECICTZ (Editorial Committee for Comprehensive Investigation of Coastal Zone and Tidal flat Resouces, Zhejiang Province), 1988. Comprehensive investigation of coastal zone and tidal flat resources. Zhejiang Province. China Ocean Press, Beijing. 485pp (in Chinese).
Edmonds, D.A., Slingerland, R.L., 2010. Significant effect of sediment cohesion on delta morphology. Nat. Geosci. 3, 105–109.
Feng, Y., Li, Y., Xie, Q., Zhang, L., 1990. The geomorphic features and interfacial activities in Hangzhou Bay. Acta Oceanolog. Sin. 12, 213–223 (in Chinese).
Flemming, B.W., Schubert, H., Hertweck, G., Müller, K., 1992. Bioclastic tidal-channel lag deposits: a genetic model. Senckenb. Marit. 22, 109–129.
Friedrichs, C.T., Aubrey, D.G., 1988. Non-linear tidal distortion in shallow well mixed estuaries: a synthesis. Estuarine Coastal Shelf Sci. 27, 521–545.
Friedrichs, C.T., Aubrey, D.G., 1994. Tidal propagation in strongly convergent channels. J. Geophys. Res. 99 (C2), 3321–3336.
Galloway, W.E., 1975. Process framework for describing the morphologic and stratigraphic evolution of deltaic depositional systems. In: Broussard, M.L. (Ed.), Deltas, Models for Exploration. Houston Geological Society, Houston, pp. 87–98.
Gao, S., 2007. Modeling the growth limit of the Changjiang Delta. Geomorphology 85, 225–236.
Geleynse, N., Storms, J.E.A., Stive, M.J.F., Jagers, H.R.A., Walstra, D.J.R., 2010. Modeling of a mixed-load fluvio-deltaic system. Geophys. Res. Lett. 37, L05402. doi:10.1029/2009GL042000.
Guillou, N., Chapalain, G., Thais, L., 2009. Three-dimensional modeling of tide-induced suspended transport of seabed multicomponent sediments in the eastern English Channel. J. Geophys. Res. 114, C07025. doi:10.1029/2008JC004791.
Guo, Y., Zhang, J., Zhang, L., Shen, Y., 2009. Computational investigation of typhoon-induced storm surge in Hangzhou Bay, China. Estuarine Coastal Shelf Sci. 85, 530–536.
Han, Z.C., Dai, Z.H., Li, G.B., 2003. Regulation and Exploitation of Qiantang River Estuary. China Water Publication, Beijing. 554pp (in Chinese with an English abstract).
Harris, P.T., 1988. Large scale bedforms as indicators of mutually evasive sand transport and the sequential infilling of wide-mouthed estuaries. Sediment. Geol. 57, 273–298.
Harris, P.T., Collins, M.B., 1985. Bedform distributions and sediment transport paths in the Bristol Channel and Severn Estuary, U.K. Mar. Geol. 62, 153–166.
Harris, P.T., Hughes, M.G., Baker, E.K., Dalrymple, R.W., Keene, J.B., 2004. Sediment transport in distributary channels and its export to the pro-deltaic environment in a tidally-dominated delta: Fly River, Papua New Guinea. Cont. Shelf Res. 24, 2431–2454.
Hibma, A., De Vriend, H.J., Stive, M.J.F., 2003a. Numerical modelling of shoal pattern formation in well-mixed elongated estuaries. Estuarine Coastal Shelf Sci. 57, 981–991.
Hibma, A., Schuttelaars, H.M., Wang, Z.B., 2003b. Comparison of longitudinal equilibrium profiles of estuaries in idealized and process-based models. Ocean Dyn. 53, 252–269.
Hori, K., Saito, Y., Zhao, Q., Cheng, C., Wang, P., Sato, Y., Li, C., 2001. Sedimentary facies of the tide-dominated paleo-Changjiang (Yangtze) estuary during the last transgression. Mar. Geol. 177, 331–351.
Kunte, P.D., Zhao, C., Osawa, T., Sugimori, Y., 2005. Sediment distribution study in the Gulf of Kachchh, India, from 3D hydrodynamic model simulation and satellite data. J. Mar. Syst. 55, 139–153.
Lanzoni, S., Seminara, G., 2002. Long-term evolution and morphodynamic equilibrium of tidal channels. J. Geophys. Res. 107 (C1), 3001. doi:10.1029/2000JC000468.
Lesser, G.R., Roelvink, J.A., van Kesteren, J.A.T.M., Stelling, G.S., 2004. Development and validation of a three-dimensional morphological model. Coast. Eng. 51, 883–915.
Lin, C.-M., Zhuo, H.-C., Gao, S., 2005. Sedimentary facies and evolution in the Qiantang River incised valley, eastern China. Mar. Geol. 219, 235–259.
Mackin, J.H., 1948. Concept of the graded river. Geol. Soc. Am. Bull. 59, 463–512.
Mao, H., Gan, Z., Shen, H., 1964. A preliminary study of the tidal flushing in Hangchow bay (I) Upper estuary. Oceanol. Limnol. Sin. 6, 121–133 (in Chinese with an English abstract).
McCave, I.N., Hall, I.R., 2006. Size sorting in marine muds: processes, pitfalls, and prospects for paleoflow-speed proxies. Geochem. Geophys. Geosyst. 7, Q10N05. doi:10.1029/2006GC001284.
Montano, Y., Carbajal, N., 2008. Numerical experiments on the long-term morphodynamics of the Colorado River Delta. Ocean Dyn. 58, 19–29.
Orton, G.J., Reading, H.G., 1993. Variability of deltaic processes in terms of sediment supply, with particular emphasis on grain size. Sedimentology 40, 475–512.
Pan, C., Huang, W., 2010. Numerical modeling of suspended sediment transport in Qiantang River: an estuary affected by tidal bore. J. Coast. Res. 26, 1123–1132.

Paola, C., 2011. Simplicity versus complexity. Nature 469, 38–39.
Peakall, J., Ashworth, P., Best, J., 2007. Meander-bend evolution, alluvial architecture, and the role of cohesion in sinuous river channels: a flume study. J. Sediment. Res. 77, 197–212.
Perillo, G.M.E., 1995. Definitions and geomorphologic classifications of estuaries, In: Perillo, G.M.E. (Ed.), Geomorphology and Sedimentology of Estuaries, 2nd Edition. : Developments in Sedimentology, 53. Elsevier Science, Amsterdam, pp. 17–47.
Prandle, D., 2004. How tides and river flows determine estuarine bathymetries. Prog. Oceanogr. 61, 1–26.
Ramaswamy, V., Nagender Nath, B., Vethamony, P., Illangovan, D., 2007. Source and dispersal of suspended sediment in the macro-tidal Gulf of Kachchh. Mar. Pollut. Bull. 54, 708–719.
Ranasinghe, R., Swinkels, C., Luijendijk, A., Roelvink, D., Bosboom, J., Stive, M., Walstra, D., 2011. Morphodynamic upscaling with the MORFAC approach: dependencies and sensitivities. Coast. Eng. 58, 806–811.
Reed, C., Niedoroda, A.W., Swift, D.J.P., 1999. Modeling sediment entrainment and transport processes limited by bed armouring. Mar. Geol. 154, 143–154.
Roelvink, J.A., 2006. Coastal morphodynamic evolution techniques. Coast. Eng. 53, 177–187.
Schumm, S.A., Khan, H.R., 1972. Experimental study of channel patterns. Geol. Soc. Am. Bull. 83, 1755–1770.
Schuttelaars, H.M., de Swart, H.E., 2000. Multiple morphodynamic equilibrium in tidal embayment. J. Geophys. Res. 105, 24105–24118.
Soulsby, R.L., 1997. Dynamics of Marine Sands. Thomas Telford, Oxford. 249 pp.
Stanley, D.J., Warne, A.G., 1994. Worldwide initiation of Holocene marine deltas by deceleration of sea level rise. Science 265, 228–231.
Su, J., Wang, K., 1989. Changjiang river plume and suspended sediment transport in Hangzhou Bay. Cont. Shelf Res. 9, 93–111.
Swift, D.J.P., Thorne, J.A., 1991. Sedimentation on continental margins: I. A general model for shelf sedimentation. In: Swift, D.J.P., Tillman, R.W., Oertel, G.F., Thorne, J.A. (Eds.), Shelf Sand and Sandstone Bodies, Geometry, Facies and Sequence Stratigraphy: International Association of Sedimentologists Special Publication, 14, pp. 3–31.
Tal, M., Paola, C., 2010. Effects of vegetation on channel morphodynamics: results and insights from laboratory experiments. Earth Surf. Process. Landforms 35, 1014–1028.
Todeschini, I., Toffolon, M., Tubino, M., 2008. Long-term morphological evolution of funnel-shape tide-dominated estuaries. J. Geophys. Res. 113, C05005. doi:10.1029/2007JC004094.
Toffolon, M., Crosato, A., 2007. Developing macroscale indicators for estuarine morphology: the case of the Scheldt estuary. J. Coast. Res. 23, 195–212.
van der Molen, J., Bolding, K., Greenwood, N., Mills, D.K., 2009. A 1-D vertical multiple grain size model of suspended particulate matter in combined currents and waves in shelf seas. J. Geophys. Res. 114, F01030. doi:10.1029/2008JF001150.
van der Wegen, M., 2010. Modeling Morphodynamic Evolution in Alluvial Estuaries (Phd Dissertation). CRC Press, Balkema. 187 pp.
Van der Wegen, M., Dastgheib, A., Jaffe, B.E., Roelvink, J.A., 2011. Bed composition generation for morphodynamic modeling: case study of San Pablo Bay in California, USA. Ocean Dyn. 61, 173–186.
van der Wegen, M., Roelvink, J.A., 2008. Long-term morphodynamic evolution of a tidal embayment using a two-dimensional, process-based model. J. Geophys. Res. 113, C03016. doi:10.1029/2006JC003983.
van der Wegen, M., Wang, Z.B., Savenije, H.H.G., Roelvink, J.A., 2008. Long-term morphodynamic evolution and energy dissipation in a coastal plain tidal embayment. J. Geophys. Res. 113, F03001. doi:10.1029/2007JF000898.
van Rijn, L.C., 2000. General view on sand transport by currents and waves. Rep. No. Z2899.20-Z2099.30-Z2824.30, Delft Hydraulics. Delft, The Netherlands.
Wells, J.T., 1995. Tide-dominated estuaries and tidal rivers, In: Perillo, G.M.E. (Ed.), Geomorphology and Sedimentology of Estuaries, 2nd Edition. : Developments in Sedimentology, 53. Elsevier Science, Amsterdam, pp. 179–205.
Whitehouse, R., Soulsby, R., Roberts, W., Mitchener, H., 2000. Dynamics of Estuarine Mud. Thomas Telford, London. 210 pp.
Wiberg, P.L., Drake, D.E., Cacchione, D.A., 1994. Sediment suspension and bed armouring during high bottom stress events on the northern California inner continental shelf: measurements and predictions. Cont. Shelf Res. 14, 1191–1219.
Xie, D., Wang, Z.B., Gao, S., de Vriend, H.J., 2009. Modeling the tidal channel morphodynamics in a macro-tidal embayment, Hangzhou Bay, China. Cont. Shelf Res. 29, 1757–1767.
Yu, Q., Wang, Y., Flemming, B., Gao, S., in press. Modeling the equilibrium hypsometry of back-barrier tidal flats in the German Wadden Sea (southern North Sea). Continental Shelf Research doi: 10.1016/j.csr.2011.05.011.
Zhou, X., Gao, S., 2004. Spatial variability and representation of seabed sediment grain sizes: an example from the Zhoushan - Jinshanwei transect, Hangzhou Bay, China. Chin. Sci. Bull. 2004, 2503–2507.